International Journal of Academic Scientific Research
ISSN: 2272-6446 Volume 7, Issue 4 (November - December2019), PP 28- 41
www.ijasrjournal.org

Evaluating energy saving and thermal comfort using a hybrid personal ventilation system

Mohammad Youssef Al Hashem[1], Ahmad Habib[2]

[1, 2] *Department of Power Engineering, Faculty of Mechanical Engineering, University of Aleppo*

Abstract: *The Increasing energy demands in buildings sector resulted in more energy saving needs, building sector consumes about 40 % of the global energy yield. Due to the modern work lifestyle, people spend more and more time inside buildings, where the ratio of spent time inside buildings reaches 86%. In this work, a hybrid personal ventilation system was proposed, combining the benefits of the standard personal ventilation, PV, and the local exhaust ventilation for offices, LEVO. The free open-source CFD software OpenFOAM was used to perform the CFD calculations in the in-doors environments. A valid numerical an experimental cubicle model was used. The local exhausts were introduced in the cubicle, and the effect of exhaust location and basic flow parameters were studied numerically. Then the numerical results were validated experimentally, the relative errors didn't exceed 1.2 % while validating the temperature flow field. Using this concept, an energy saving of 13.53% was accomplished compared to a standard personal ventilation system. Economical operation conditions that can save about 46.74% from the consumed energy and keep an acceptable comfort level compared to the best available thermal conditions were determined.*

Keywords: *Age of air, OpenFOAM, personal ventilation, thermal comfort, thermal plume.*

1. INTRODUCTION

1.1. Background

Due to the modern work lifestyle, people spend the majority of their time indoors [1-3]. Therefore, human thermal comfort should be maintained at a high level. In recent decades, various ventilation methods and devices have been developed to provide a comfortable thermal environment for occupants and to reduce the demand for energy [4-7].

One of the most important methods is to use the Personalized Ventilation systems (PV), where the cool and fresh air is supplied directly to each person's breathing zone in the conditioned area [8], then, the return air is collected form the conditioned area using a normal ventilation method. In addition, a Local Exhaust Ventilation (LEV) also called the Personalized Exhaust (PE) system can be used to improve the thermal comfort. In this system, warm and contaminated air is extracted locally before reaching the occupied area, which consequently enhances the quality of the inhaled air. The LEV system is used to control the contaminant transmission in occupied areas [9-12] and has been widely used in industrial applications to provide a healthy and comfortable work space.

Ahmed et al. [13] performed a numerical investigation for a Local Exhaust Ventilation for Office (LEVO) system. The result shows that the new local exhaust ventilation system can reduce the energy consumption by up to 30%, compared with an office not using this system. Furthermore, this system was able to reduce the contaminant concentration in a micro-environment area by up to 61% and improve the human thermal comfort in the occupied zone. Taheri et al. [14] conducted a field study concerning indoor conditions in an office. The office is equipped with displacement ventilation (DV) as well as personal ventilation (PV) systems. The results suggest that the combined operation of the above mentioned systems provides in general acceptable indoor environmental conditions. Kong et al [15] conducted a numerical investigation to build an appropriate computational fluid dynamics (CFD) model for simulating the flow field in the office cubicle with and without personalized ventilation (PV) and using it to investigate the flow field in the cubicle. A brief evaluation of the environmental quality was conducted for both cases with PV and under floor air diffuser (UFAD). This comparison showed a

significant advantage in the PV system, indicating how the PV system performed under different airflow rates. Melikov et al. [16] used an LEV concept to develop the thermal environment around a hospital bed and investigated the reduction of the exposure for the doctor and the patient with and without the LEV system. They found that with the LEV system the exposure level was reduced significantly for people who sat close to the patient. Dygert and Dang [10] proposed to use a local exhaust suction device in an airplane, and their results showed that up to 90% reduction of exposure to contamination comes from other passengers. Furthermore, they concluded that this type of LEV is suited to a high density occupation. Zítek et al. [12] investigated the thermal environment and the air quality around the occupants in an aircraft using a separate air flow supply and a separate local exhaust. Their results showed that using this system protected the occupants from possible dispersion of disease in an aircraft environment.

1.2. Purpose

The previous studies focused on using the PV systems in offices spaces with a normal air return system. Or using a LEV system in offices rooms, hospitals rooms, airplanes and on some industrial applications to improve the quality of the inhaled air and provide a healthy and comfortable environment for the occupants. However, no study had considered the PV as a ventilation system in an office space combined with LEVO system. In this research, a hybrid personal ventilation system for a cubicle was proposed, combining the benefits of the standard personal ventilation systems PV and the local exhaust ventilation for office (LEVO) systems. On the other hand, the commercial CFD codes – beside its high costs – aren't easily available in some countries. Also the open-source CFD codes are getting widely used in all research fields. The free open-source CFD software OpenFOAM was used to perform the CFD calculations in the indoor environments.

2. Method and procedure

2.1. Overview

The main cubicle prototype used in this research was proposed by Al Hashem and Habib in [17], this model was able to predict the physical phenomena in an office cubicle and calculate the thermal comfort quantities correctly.

The numerical model was validated after performing a mesh independence study by comparing its basic flow parameters with valid numerical results, and the experimental model was also validated by comparing its results with experimental results.

The prototype is an office room (1150 cm × 450 cm × 300 cm) with one cubicle that has the same dimensions (191×184×171 cm with a 84 cm door opening) and features as in [15], located at Aleppo University – Faculty of Mechanical Engineering.

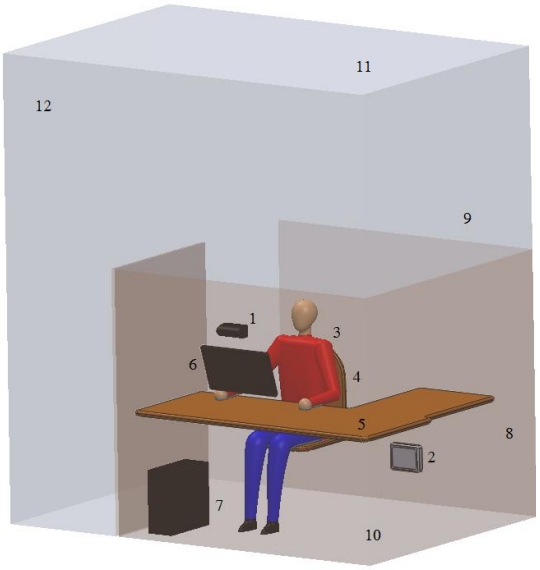

Fig.1 Cubicle configuration.

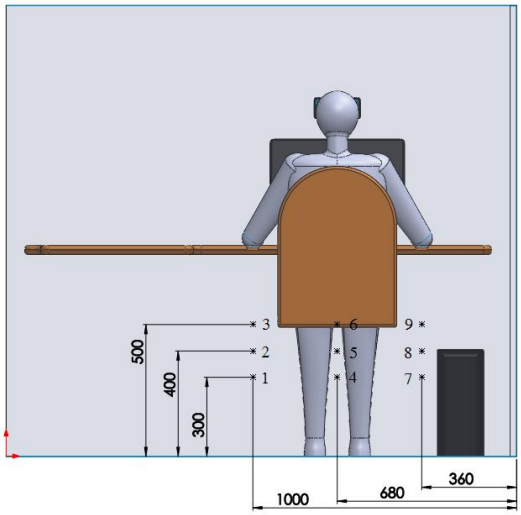

Fig. 2 Exhaust locations.

The used cubicle configuration is shown in (Fig. 1). It contains the 1- supply vent, 2- exhaust, 3- seated manikin, 4- chair, 5- table, 6- monitor, 7- computer case, 8- cubicle partitions, 9- office wall, 10- floor, 11- celling and 12- symmetry planes.

The local exhaust was introduced in the cubicle, and in order to investigate the effect of local exhaust extensively, nine exhaust locations were chosen (Fig. 2). Exhaust locations concentrated at the lower zone behind the manikin at 10 cm from the rear partition.

The flow fields and the thermal comfort indicators were recorded during the numerical simulations on three vertical lines along the cubicle in the locations A, B and C (Fig.3), noting that the location C is mobile according to the exhaust location.

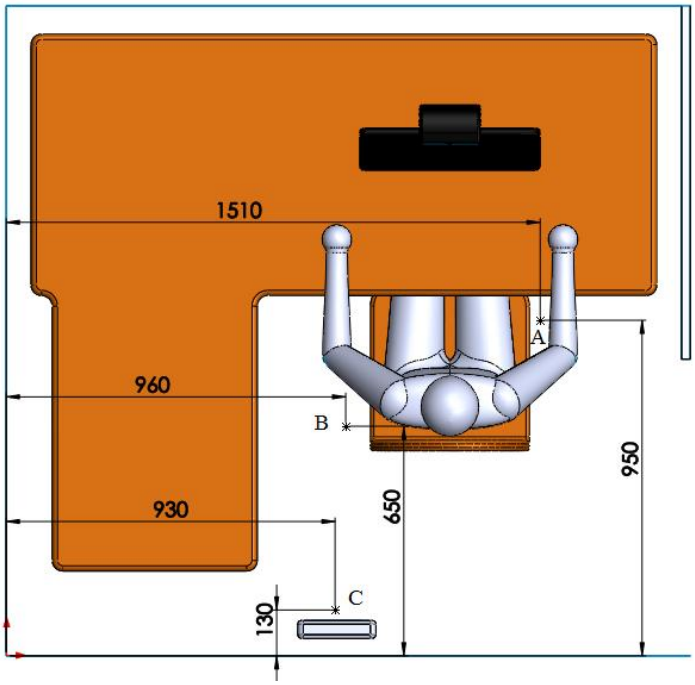

Fig.3 Data monitoring locations.

The cubicle has a supply vent connected to circular duct with a diameter of 7.5 cm, the supply vent's main dimensions are (7.4 cm × 16.4 cm) and it contains 6 horizontal blades and 10 vertical blades with actual area of 0.008496 m^2. The supply vent is located at 135 cm above the floor and 34 cm away from the front partition (Fig. 4).

Fig.5: The supply vent

2.2. Experiment setup

All the numerical simulation had been reconstructed experimentally to validate its results. The experimental model constructed in [17] was used in these experiments, and the temperature controllers mentioned in [17] had been used to monitor the temperature field during the experiments, 18 temperature sensors had been distributed in the locations A, B and C in addition to one sensor for the return air temperature and one sensor for the supply air temperature.

The used temperature controllers type is Cheng KE CK-002, and the sensors are NTC type (Negative Temperature Coefficient) with accuracy of ∓ 0.5 ℃ and sensitivity of 0.1 ℃ [17]. The desired flow rate was determined using the supply vent's actual area and the average air velocity at the vent, a hand held anemometer type CFM model 8901 was used to measure the average air velocity at the supply vent. The anemometer accuracy was $\mp 2\%$ and had the sensitivity of 0.01 $[m/s]$.

Each experiment started after 15 minutes of operation and the temperature measurement was taken three times with 5 minutes in between, then the average reading was used. Instead of using a sophisticated thermal manikin, a real average shaped and average metabolic rate male with normal summer clothing (1.2 met, 0.6 col) was used in our experiments. The subject was in a comfortable situation during the experiments.

2.3. Governing equations for CFD model

As in [17], the eddy-viscosity RANS model was used. The basic equations include the transport equation of mass, momentum, and other quantities.

$$\frac{\partial}{\partial x_i}(\rho u_i) = 0 \tag{1}$$

$$\frac{\partial}{\partial t}(\rho u_j) + \frac{\partial}{\partial x_i}(\rho u_i u_j) = -\frac{\partial p}{\partial x_j} + \frac{\partial}{\partial x_i}\left(\mu \frac{\partial u_i}{\partial x_i} - \rho\overline{u_j' u_i'}\right) + S_j \tag{2}$$

$$\frac{\partial}{\partial t}(\rho\phi) + \frac{\partial}{\partial x_i}(\rho u_i \phi) = \frac{\partial}{\partial x_i}\left(\Gamma \frac{\partial f}{\partial x_i} - \rho\overline{u_i'\phi'}\right) + S \tag{3}$$

Boussinesq and Reynolds' analogies are used to model the turbulent term.

$$\tau_{ij} = -\rho\overline{u_j' u_i'} = \mu_t \frac{\partial u_i}{\partial x_i} \tag{4}$$

$$H_i = \rho C_p \overline{u_i' T^i} = -\rho C_p \nu_t \frac{\partial T}{\partial x_i} \tag{5}$$

Also in this paper, the $realizable\ k-\varepsilon$ turbulence model was used. This turbulence model had proved to be able to predict the indoor environment flow characters correctly [17]. This model have an advantage on the $standard\ k-\varepsilon$ model by using the two-layer approach, developed by [18], this approach is used as an alternative to the low- Reynolds' number approach that allows the one-equation turbulence model to be applied in the near-wall region and the two-equation $k-\varepsilon$ model to be applied in the region away from the wall. With this approach, the whole flow field is divided into two regions, the near-wall layer and the far-field. In the near-wall layer, the turbulent kinetic energy k is calculated by

$$\frac{\partial k}{\partial t} + u_i \frac{\partial k}{\partial x_i} = d_k + P_k + G_k - \varepsilon \tag{6}$$

The eddy viscosity is calculated by

$$\nu_t = \sqrt{\overline{u'u'}}\, l_\mu \tag{7}$$

The turbulence dissipation rate ε by

$$\varepsilon = \frac{\sqrt{\overline{u'u'}}\, k}{l_\varepsilon} \tag{8}$$

Where G_k is the gravity production of turbulent kinetic energy, P_k is the shear production of the turbulent kinetic energy, and l_μ and l_ε are characteristic lengths that are defined in [19].

The values of ε specified in the near-wall layer are blended smoothly with the values computed from solving the $k-\varepsilon$ equations far from the wall. The equation for turbulent kinetic energy is solved in the entire flow. This explicit specification of ε and μ_t is arguably no less empirical than the low-Reynolds' number approach, and the results are often better or comparable to the $standard\ k-\varepsilon$ results. In OpenFOAM, the two-layer formulations will work with either low-Reynolds' number type meshes $y^+ \sim 1$ or wall-function type meshes $y^+ > 30$ [20].

2.4. Post processing

In order to quantify the thermal comfort status, several comfort indicators are available. An additional library had been added to the software code to calculate these indicators, this library (comfortFoam) was used to analyze the thermal comfort behavior based on EN ISO 7730 [21], and to calculates the predicted mean vote (PMV), predicted percentage of dissatisfaction (PPD), clothing temperature (T_{cl}), the mean radiant temperature T_{MR} and the age of air (AoA).

The predicted mean vote (PMV) was first proposed by Fanger [22], which can be represented on the ASHRAE 7-points thermal sensation scale, given in table 1. Fanger's PMV correlation is based on the identification of a skin temperature and sweating rate required for the optimal comfort conditions. The predicted percentage of dissatisfaction (PPD) has a greater sensitivity for air velocity and is calculating based on the PMV values using eq. 9 [22].

Table.1: ASHRAE 7-points thermal sensation scale

Value	Sensation
-3	Cold
-2	Cool
-1	Slightly cool
0	Neutral
1	Slightly warm
2	Warm
3	Hot

$$PPD = 100 - 95 \cdot \exp\left(-a_p \cdot PMV^4 - b_p \cdot PMV^2\right) \quad (9)$$

In order to assess the ventilation effectiveness, a number of parameters or indices have been proposed, such as macro air exchange rate, air change efficiency, local air change efficiency, local ventilation index, purging air flow rate [23, 24]. Many of these parameters are associated with air age, which is generally defined as the time that has elapsed since air element enters the room [24]. A low AoA value means that the air is often renewed, implying a good air quality. Additional differential transport equation (Eq. 10) of a scalar τ which represents the AoA [25] is solved.

$$\frac{\partial \tau}{\partial t} + \frac{\partial}{\partial x_i}(u_i \tau) - \frac{\partial}{\partial x_i}\left(\frac{\nu_{eff}}{\sigma_\tau} \cdot \frac{\partial \tau}{\partial x_i}\right) = 1 \quad (10)$$

Where the term $\frac{\partial \tau}{\partial t}$ represents the accumulation over time, the term $\frac{\partial}{\partial x_i}(u_i \tau)$ represents the transport of τ by advection, the term $\frac{\partial}{\partial x_i}\left(\frac{\nu_{eff}}{\sigma_\tau} \cdot \frac{\partial \tau}{\partial x_i}\right)$ represents the diffusion of τ, and the right term is the source term which is equal to 1.

3. Results and discussion

3.1. The effect of exhaust location

To evaluate the effect of exhaust location, three CFD simulations were performed in each on the nine exhaust locations starting from the conditions used in Kong's simulations [15] given in table 2.

Table.2: The CFD simulations in each exhaust location

Simulation in each location	Supply flow rate Q $[l/s]$	Supply Temperature T_S [℃]
1	9.4	17.5
2	9.4	18.4
3	10	18.4

The volume weighted average PMV and PPD were calculated for each simulation (Fig. 6). Generally, the cubicle's thermal condition lies within the comfortable range $(-0.5 < PMV < +0.5)$ according to EN ISO 7730 [21], and the PMV and PPD values decreases by reducing the supply temperature and by increasing the supply flow rate.

The PMV values decreases slightly by increasing the exhaust height and by increasing the horizontal distance to the door. The PPD values acted similarly to the PMV values.

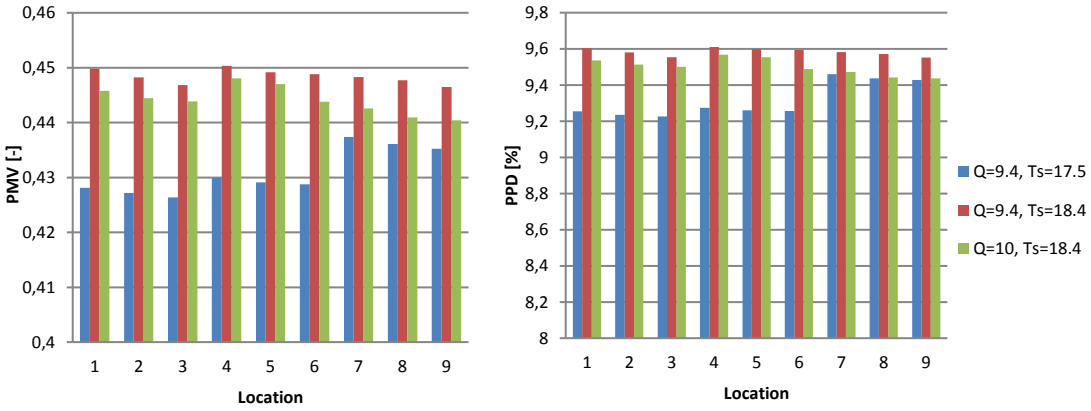

Fig. 6 PMV, PPD volume weighted average.

Also, the age of air at the outlet and the return temperature were calculated (Fig. 7). The age of the air at the outlet decreases significantly at the exhaust location 4, 5, and 6 (behind the manikin) since these locations are in the same plane as the supply vent, and increases significantly at the exhaust locations near the door.

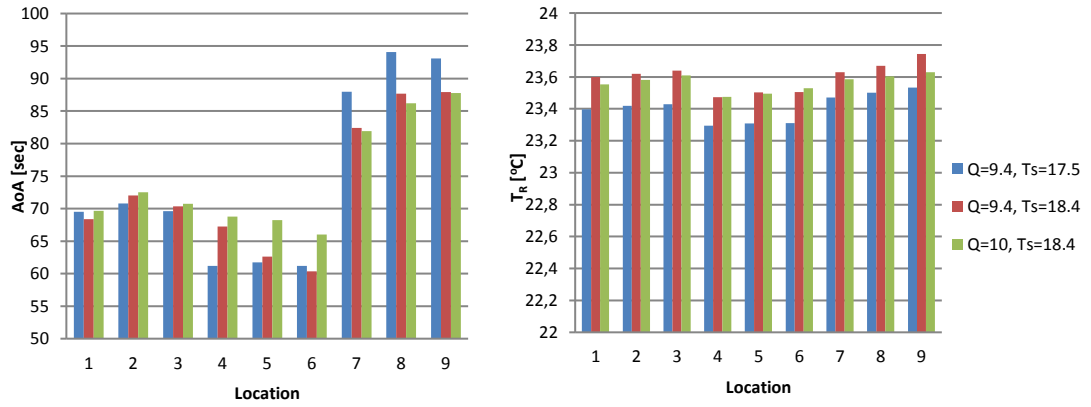

Fig. 7 AoA and return temperature.

Neither too low nor too high AoA values are preferred, since a low AoA value at the exhaust means that the air went through the cubicle from supply directly to exhaust, and a high AoA value at the exhaust means that the air had spent too much time in the cubicle and become contaminated. So, the moderate values are preferred.

The return temperature acted similarly to age of air but with much smaller differences between locations, since the air that reaches the exhaust quicker will still be colder.

3.2. The effect of flow parameters

In order to investigate the effect of flow field's parameters on the thermal conditions, the exhaust location 1 was used to carry on more CFD simulation. It was found earlier that increasing the supply flow rate and decreasing the supply temperature decreases the PMV and PPD values (closer to the complete neutral thermal conditions).

The effect of decreasing the supply temperature and increasing the supply flow rate will be investigated.

3.2.1. The effect of supply temperature

Starting from the conditions ($Q = 9.4\ l/s, T_s = 18.4$ ℃), the supply temperature was lowered to 17.5, 16.5 ℃ and the thermal indices were calculated. AoA at the outlet as shown in (Fig. 8) increases at the supply temperature 17.5 ℃ due to the increasing mixing dynamics resulted from colder leaning downward jet flow, then decreases significantly at 16.5 ℃, due to the more downward leaning colder jet flow that can reach the exhaust location quickly. The return temperature as shown in (Fig. 9) had a reasonable behavior and decreases by decreasing the supply temperature.

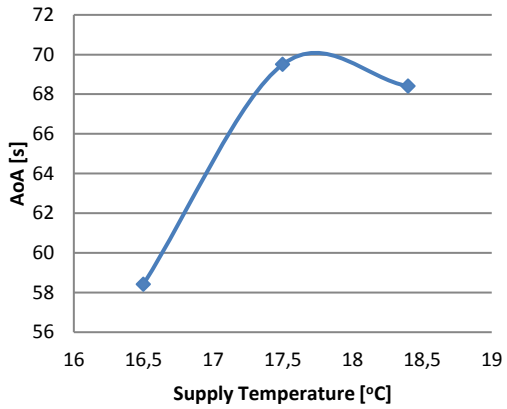

Fig. 8 AoA at the outlet

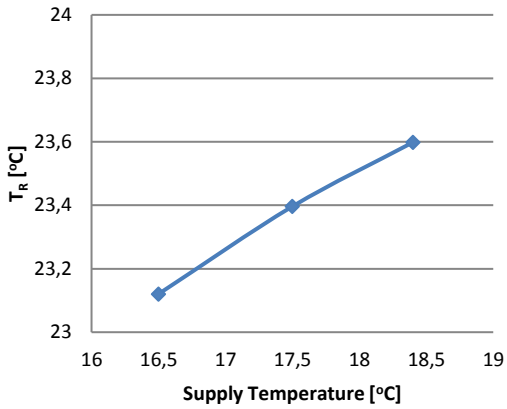

Fig. 9 Return temperature

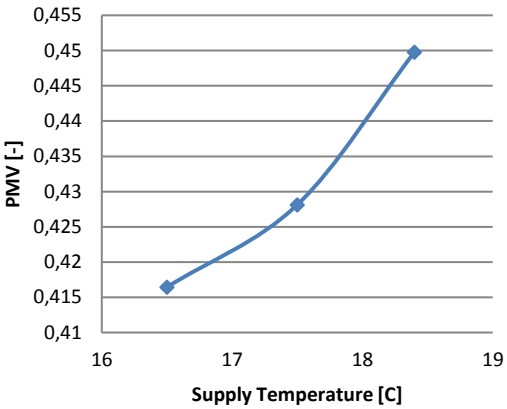

Fig. 10 Volume weighted average PMV

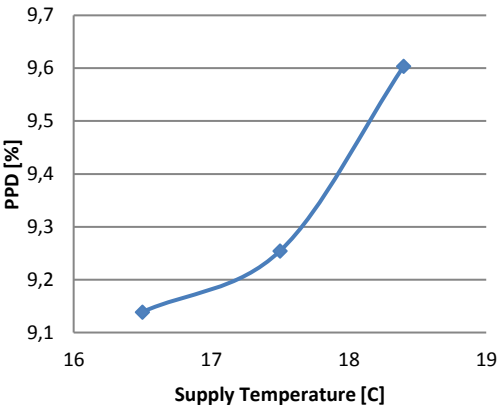

Fig. 11 Volume weighted average PPD

The volume weighted average PMV (Fig. 10) and PPD (Fig. 11) values decreased by decreasing the supply temperature, but no supply temperatures below 16.5 [℃] was examined since the supply temperatures below this value is not healthy nor recommended.

3.2.1. The effect of supply flow rate

Starting from the conditions ($Q = 9.4\ l/s, T_s = 18.4$ ℃), the supply flow rate was increased in order to obtain the best thermal conditions. AoA at the outlet (Fig. 12) shows an increasing in the AoA values by increasing the supply flow rate due to the complications of the mixing dynamics, followed by a rapid decrease at the higher flow rates values because the faster the jet flow can reach the exhaust zone much quicker.

The volume weighted average PMV (Fig. 14) and PPD (Fig. 15) values decrease by increasing the supply flow rate up to $18\ [l/s]$, and then the slope of the volume weighted average PMV curve degreases while the volume weighted average PPD starts to increase by increasing the supply flow rate. This happened due to the higher air velocities at the higher flow rates, which still produce comfortable thermal conditions according to the PMV indicator will then produce unpleasant thermal conditions according to the PPD indicator because its higher sensitivity to the air velocity.

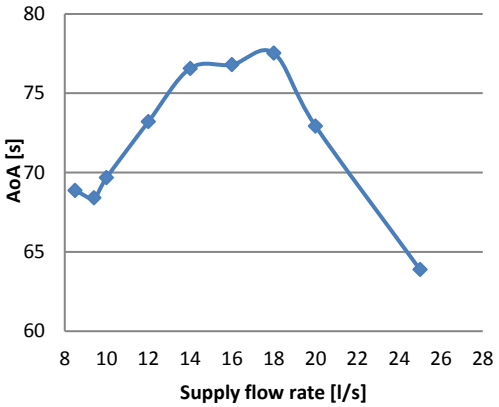

Fig. 12 AoA at the outlet

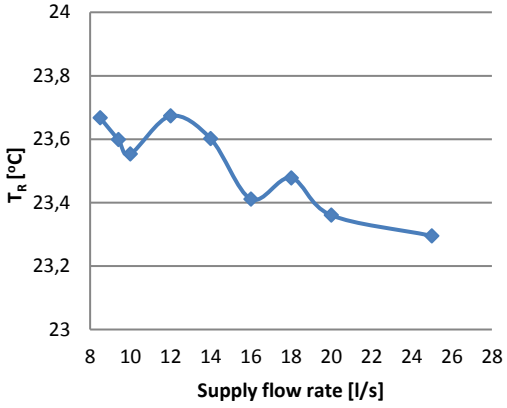

Fig. 13 Return temperature

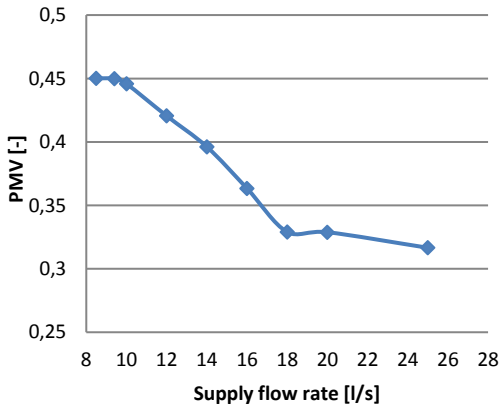

Fig. 14 Volume weighted average PMV

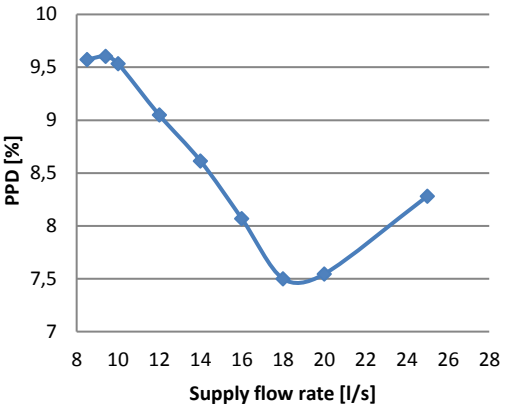

Fig. 15 Volume weighted average PPD

This phenomenon can be explained further more by reviewing the PMV contours (Fig. 16) and the PPD contours (Fig. 17) in the manikin plane at the mid and high air flow rates.

It can be seen that at the higher flow rates, the heat plume forms vividly around the body and the PMV and PPD values rises significantly on the body, caused by the high velocity supply jet flow, which acts as an aerial curtain blocking the heat plume from rising and the cool and clean air stays at the face area.

So the thermal conditions at $Q = 18\ l/s\ , T_s = 18.4\ ℃$ could be considered to be the best thermal conditions that could be achieved.

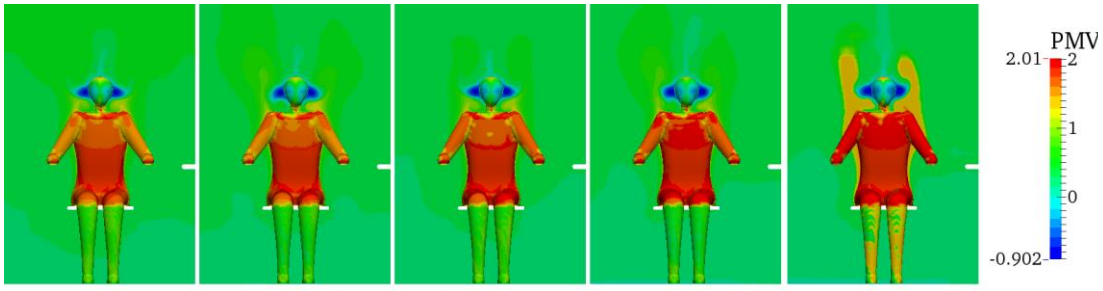

14 $[l/s]$ **16 $[l/s]$** **18 $[l/s]$** **20 $[l/s]$** **25 $[l/s]$**

Fig. 16 PMV contours.

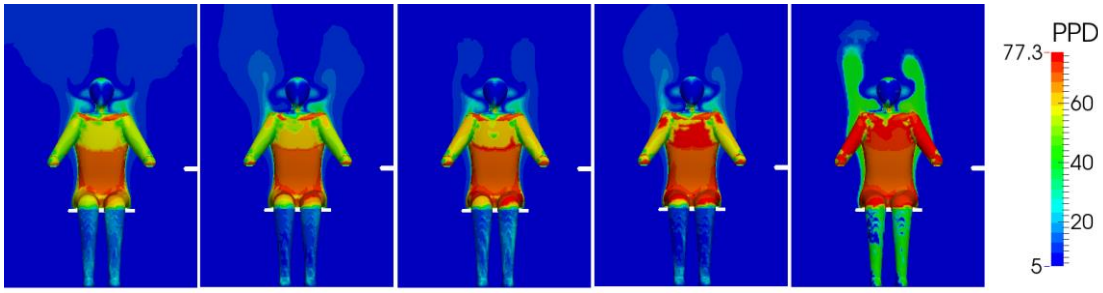

14 $[l/s]$ **16 $[l/s]$** **18 $[l/s]$** **20 $[l/s]$** **25 $[l/s]$**

Fig. 17 PPD contours.

3.3. Validating the numerical results

The average relative error in the temperature field at each monitoring location was calculated in each experiment, in addition to the return air temperature relative error. The average relative errors of the experiment with a constant supply temperature are shown in (Fig. 18) and the average relative errors of the experiment with a constant supply flow rate are shown in (Fig. 19).

The relative errors of the numerical simulations were around 1.2 % compared to the experiments, and due to the importance of temperature field in calculating the thermal comfort indices, the numerically calculated thermal comfort indices can be considered to be valid.

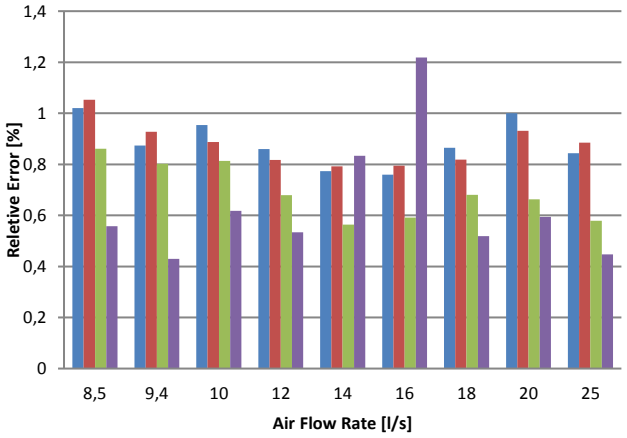

Fig. 18 Relative error at constant supply temperature.

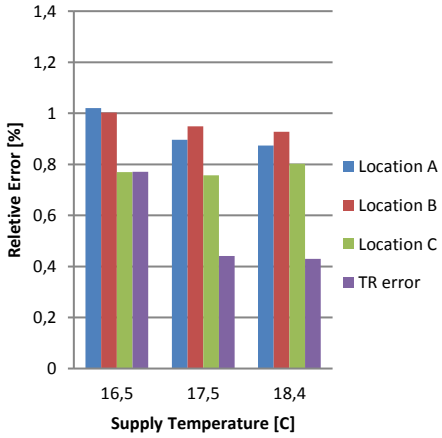

Fig. 19 Relative error at constant supply flow rate.

3.4. Evaluating energy consumption and thermal comfort

The main purpose of using personalized ventilation system is energy savings and improving the thermal conditions. In HVAC systems, energy is consumed mainly in air handling (cooling, heating, etc.) and air delivering system. Cooling power can be calculated by eq. 11.

$$P_c = \dot{m} \cdot (h_R - h_S)\ [W] \tag{11}$$

The return and supply enthalpies $h_R,\ h_S$, the mass flow rate $\dot{m}$ is calculated using eq. 12.

$$\dot{m} = \left(\frac{\rho_S + \rho_R}{2}\right) \cdot Q\ [kg/s] \tag{12}$$

The supply and return air densities are $\rho_S,\ \rho_R$, air densities and enthalpies were obtained using psychrometric chart. Fan power is calculated using eq. 13, where the pressure difference on the fan Δp, is calculated using eq. 14, $\rho_w = 1000\ [kg/m^3]$ is the density of fluid (water) used in the differential barometer shown in (Fig. 20) and H is the difference between water surfaces in the barometer. Then the total consumed power is calculated using eq. 15.

$$P_f = \Delta p \cdot Q\ [W] \tag{13}$$

$$\Delta p = \rho_w \cdot g \cdot H\ [Pa] \tag{14}$$

$$P = P_c + P_f\ [W] \tag{15}$$

Fig. 20 The differential barometer

3.4.1. Energy savings

In this paper, a hybrid personal ventilation system that combines the benefits of the standard PV systems and the LEVO systems was proposed. In order to evaluate the energy savings associated with this hybrid system, a comparison in cooling power between this system and a standard personal ventilation system applied to an identical cubicle at the same thermal conditions [15] was done.

The comparison was confined on the cooling power due to the lack of information about air delivering system, table 3 shows the comparison in the cooling power between a standard and the proposed hybrid PV system, power consumption. The results show that the cooling power was reduced by 13.53 %.

Table.3: Comparing the cooling power between a standard and the hybrid PV system.

	Supply temperature T_S [℃]	Return temperature T_R [℃]	Air flow rate Q $[l/s]$	Cooling power P_c $[W]$
Standard PV [15]	18.4	24.5	9.4	155.82
Hybrid PV	18.4	23.7	9.4	134.74
The reduction in power consumption				13.53 %

3.4.2. Choosing the operation conditions

According to the numerical simulations, the best thermal conditions that could be obtained from the hybrid PV system accomplished at ($Q = 18\ l/s$, $T_S = 18.4$ ℃). Comfortable conditions could be achieved at economic conditions. Table 4 provides a comparison between the best thermal conditions and economic conditions in terms of the power consumption and the PMV volume weighted average. Economic conditions were selected with a high supply temperature and a low supply flow rate (reducing cooling and fan power) with an acceptable air velocity at the target.

Application of the economic condition yields a reduction in power of $118.57\ [W]$, which corresponds with a 46.74 % energy savings. On the other hand, the volume weighted average PMV still lies within the acceptable PMV rang ($-0.5 < PMV < +0.5$) according to EN ISO 7730 [21].

Table.4: The CFD simulations in each exhaust location

	Air flow rate Q $[l/s]$	Supply temperature T_S [℃]	Power P $[W]$	PMV volume weighted average
Best thermal conditions	18	18.4	253.680	0.3290
Economic conditions	9.4	18.4	135.108	0.4498

The thermal conditions at the considered operation conditions could be evaluated furthermore using the concept of equivalent temperature (T_{eq}), which is defined according to ISO 14505-2 [26] as "the temperature of a homogeneous space with the mean radiant temperature equal to air temperature and zero air velocity, in which a person exchanges the same heat loss by convection and radiation as in the actual conditions under assessment", and the summer comfort zones proposed by Nilsson and Hakan [27]. Fig. 21 shows the calculated equivalent temperature in the summer comfort zones for both operation conditions.

Both the considered operation conditions lie within the neutral comfort zone, and most of the body part had good T_{eq} values, except for the thighs which lie in the "hot but comfortable" zone.

The thermal conditions did not improve while operating on the best thermal conditions compared with the economic conditions. So, operating with the best thermal conditions is not justified, especially with the enormous amount of energy savings corresponded with operating on the economic conditions.

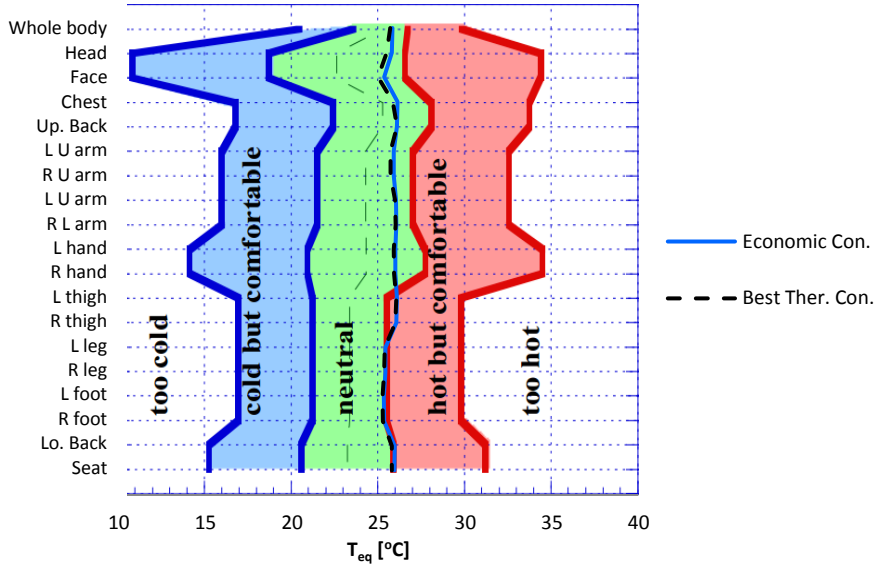

Fig. 21 Summer comfort zones for the economic and the best thermal conditions.

3.5. Uncertainty analysis

A high precision method of estimating the uncertainty in experimental results has been presented by Kline and McClintock [28]. The method is based on a careful specification of the uncertainties in the various primary experimental measurements. An uncertainty analysis of the calculated total power was performed in this section. The total power in eq. 16 is a function of the parameters $x_1, x_2, x_3, \cdots x_n$, then the absolute uncertainty in the total power is estimated using eq. 17, where w_1 is the uncertainty of variable x_1 and so on.

$$P = P(x_1, x_2, x_3, \cdots x_n) \tag{16}$$

$$w_P = \sqrt{\left(\frac{\partial P}{\partial x_1} w_1\right)^2 + \left(\frac{\partial P}{\partial x_2} w_2\right)^2 + \cdots + \left(\frac{\partial P}{\partial x_n} w_n\right)^2} \tag{17}$$

The absolute uncertainties in the consumed power at each calculation point are shown on the power curves with constant supply flow rate (Fig. 22) and the power curves with constant supply temperature (Fig. 23). The relative uncertainty of the consumed power was around 3 % for all cases.

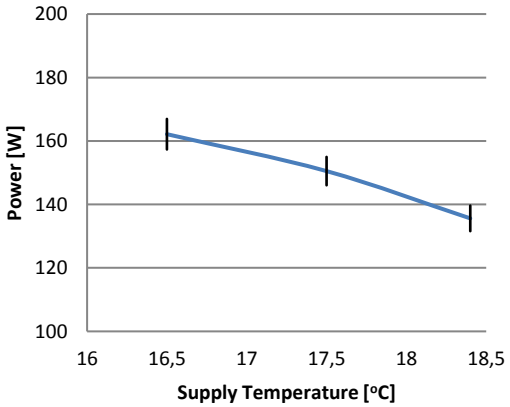

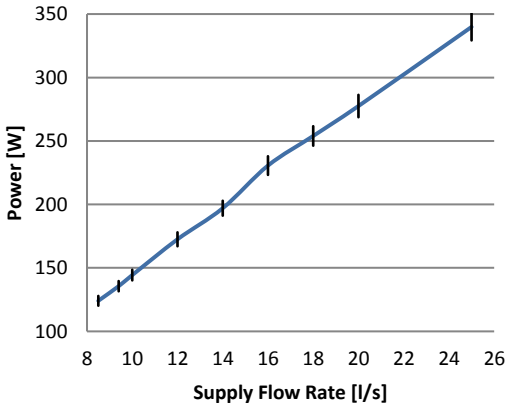

Fig. 22 Power at constant supply flow rate

Fig. 23 Power at constant supply temperature

4. CONCLUSION

In this paper, a hybrid personal ventilation system was proposed combining the benefits of the standard personal ventilation systems and the local exhaust ventilation in offices. The system was simulated numerically at several exhaust location cases, in addition to investigate the effect of flow parameters on the thermal conditions. The numerical simulations were validated experimentally and the relative errors where around 1.2 %.

The suggested hybrid personal ventilation system was able to provide comfortable thermal conditions in the cubicle according to the PMV indicator and using the summer comfort zones.

A reduction in the consumed power by 13.53 % was achieved using this hybrid personal ventilation system.

5. REFERENCES

[1] Maio, S., et al., *Indoor air pollution and airway disease*, in *Allergy Frontiers: Epigenetics, Allergens and Risk Factors*. 2009, Springer. p. 387-401.
[2] Guo, H., et al., *Risk assessment of exposure to volatile organic compounds in different indoor environments.* 2004. **94**(1): p. 57-66.
[3] Klepeis, N.E., et al., *The National Human Activity Pattern Survey (NHAPS): a resource for assessing exposure to environmental pollutants.* 2001. **11**(3): p. 231.
[4] Chemisana, D., et al., *Building integration of concentrating systems for solar cooling applications.* 2013. **50**(2): p. 1472-1479.
[5] Calay, R.K. and W.C.J.A.T.E. Wang, *A hybrid energy efficient building ventilation system.* 2013. **57**(1-2): p. 7-13.
[6] Guo, Y., et al., *A techno-economic comparison of a direct expansion ground-source and a secondary loop ground-coupled heat pump system for cooling in a residential building.* 2012. **35**: p. 29-39.
[7] Fong, K., et al., *Effect of neutral temperature on energy saving of centralized air-conditioning systems in subtropical Hong Kong.* 2010. **30**(13): p. 1659-1665.
[8] Melikov, A.K.J.I.a., *Personalized ventilation.* 2004. **14**: p. 157-167.
[9] Dygert, R.K., T.Q.J.B. Dang, and Environment, *Mitigation of cross-contamination in an aircraft cabin via localized exhaust.* 2010. **45**(9): p. 2015-2026.
[10] Dygert, R.K., T.Q.J.B. Dang, and Environment, *Experimental validation of local exhaust strategies for improved IAQ in aircraft cabins.* 2012. **47**: p. 76-88.
[11] Melikov, A.K., Z.D. Bolashikov, and M. Brand. *Experimental investigation of performance of a novel ventilation method for hospital patient rooms*. in *21st Congress of International Federation of Hospital Engineering (IFHE)*. 2010.
[12] Zítek, P., et al., *Novel personalized and humidified air supply for airliner passengers.* 2010. **45**(11): p. 2345-2353.
[13] Ahmed, A.Q., S. Gao, and A.K.J.A.T.E. Kareem, *Energy saving and indoor thermal comfort evaluation using a novel local exhaust ventilation system for office rooms.* 2017. **110**: p. 821-834.
[14] Taheri, M., et al. *A performance assessment of an office space with displacement, personal, and natural ventilation systems*. in *Building Simulation*. 2016. Springer.
[15] Kong, M., J. Zhang, and J. Wang. *Air and air contaminant flows in office cubicles with and without personal ventilation: A CFD modeling and simulation study*. in *Building Simulation*. 2015. Springer.
[16] Melikov, A., Z.D. Bolashikov, and E.J.P.o.i.a. Georgiev, *Novel ventilation strategy for reducing the risk of airborne cross infection in hospital rooms.* 2011. **1037**.
[17] Al Hashem, M.Y. and A. Habib, *Numerical and experimental investigations of personal ventilation system in a cubicle.* International Journal of Academic Scientific Research, 2019. **7**(3): p. 1-15.
[18] Xu, W., Q.J.E. Chen, and Buildings, *A two-layer turbulence model for simulating indoor airflow: Part II. Applications.* 2001. **33**(6): p. 627-639.
[19] Xu, W. and Q.J.I.a. Chen, *Simulation of mixed convection flow in a room with a two-layer turbulence model.* 2000. **10**(4): p. 306-314.
[20] Open, C., OpenFOAM Foundation, *OpenFOAM user guide.* 2011. **2**(1).
[21] Iso, E.J.E.o.t.t.e.-A.d., et al., *7730: 2005.* 2005.
[22] Fanger, P.O.J.T.c.A. and a.i.e. engineering., *Thermal comfort. Analysis and applications in environmental engineering.* 1970.
[23] Federspiel, C.C.J.I.A., *Air-Change Effectiveness: Theory and Calculation Methods.* 1999. **9**(1): p. 47-56.
[24] Sandberg, M., M.J.B. Sjöberg, and environment, *The use of moments for assessing air quality in ventilated rooms.* 1983. **18**(4): p. 181-197.
[25] Li, X., et al., *Total air age: an extension of the air age concept.* 2003. **38**(11): p. 1263-1269.
[26] ISO, E.J.G., *14505-2. Ergonomics of the thermal environment-Evaluation of thermal environments in vehicles-Part 2: Determination of equivalent temperature.* 2006.
[27] Nilsson, H.O., *Comfort climate evaluation with thermal manikin methods and computer simulation models*. 2004.
[28] Kline, S.J.J.M.E., *Describing uncertainty in single sample experiments.* 1953. **75**: p. 3-8.